4 Experimental Facilities

Fully capitalizing on the superlative performance of NSLS-II will require equally advanced beamlines and optimized and unique endstation instrumentation. In this section, we outline our current plans for beamlines, sample environments, automation and robotic control of beamlines and endstation hardware, and advanced detectors. In each area, there are challenges associated with utilizing the full performance of NSLS-II. For example, advances in mirror technology and nanoprobe optics, as well as advanced, efficient, high throughput, area detectors, are necessary to take full advantage of the high brightness and high flux of NSLS-II. There are a number of developments which hold great promise for providing these advanced capabilities and these are also discussed.

4.1 Beamlines

We have developed a preliminary estimate of the type and number of insertion device beamlines which will be necessary to satisfy the needs of the science programs outlined in Section 2. These are shown in Table 4.1.1 and indicate that NSLS-II will be able to support a sufficient number and variety of beamlines to support a large and diverse scientific program well matched to that described in Section 2.

We have included provision for four complete insertion device beamlines in the initial NSLS-II project, including front-ends and undulators. It is expected that the rest of the beamlines will be developed in response to scientific proposals from the user community. These proposals will be selected based on scientific merit and will define the scientific mission of a beamline and the requirements that the beamline and endstation instrumentation must meet in order to fulfill that mission. Some of these beamlines are likely to built and operated by the users but the majority is expected to be built and operated for the user community by the facility.

The science programs supported by NSLS-II have widely varying requirements for the photon energy range and control of the photon polarization. There is no single insertion device which can satisfy all of these requirements, and so it is essential that the insertion device be thought of as part of the beamline in order to provide an optimum photon spectrum. As outlined in Section 3.4.12, there are several types of insertion devices to choose from that are optimized to provide differing energy ranges and polarization capabilities. Thus, the rest of the insertion devices and associated front ends for the remaining beamlines beyond the initial four mentioned above will be included as components of the individual beamline construction projects.

Type of Beamline	**Number**	
Macromolecular Crystallography	5	
X-ray Microdiffraction	1	
Materials Science/time-resolved	1	
Resonant/Magnetic Scattering	1	
Soft X-ray	4	
Coherent X-ray Scattering	1	
Small Angle X-ray Scattering	1	
Inelastic X-ray Scattering	1	
Superconducting Wiggler (High Energy)	2	(Split into 6 tandem beamlines)
To Be Determined	4	
TOTAL	**21**	

Table 4.1.1 *Preliminary insertion device beamline plan. Each beamlines may have multiple hutches, some of which may be able to operate in tandem, simultaneously. This plan assumes a single insertion device beamline per straight section. However, the possibility of chicaning two undulators in a single straight section to provide photons to two independent beamlines per straight will also be investigated.*

4.1.1 X-ray Beamlines

4.1.1.1 X-ray Scattering/Crystallography Beamlines

The ultra-low emittance of NSLS-II in combination with 5m long 14 mm-period superconducting undulators (undulator U14) will provide a very intense and well-collimated source of X-rays that are ideal for X-ray scattering and crystallography applications. The small angular divergence of the X-ray beam emitted by NSLS-II undulators will allow the collection of the entire photon beam with a relatively compact Kirkpatrick-Baez (KB) mirror assembly. For example, at ~30 m from an undulator source, the width of the horizontal fan of X-rays will only be ~ 2.4 mm [4-σ] and an 80 cm long horizontally focusing mirror will intercept the full beam at a grazing incidence angle of 3 mrad. These optics will allow the X-rays to be focused onto small crystals that are a few tens of microns in diameter with relatively small convergence angles (<100 μrad vertically). Using typical mirror coatings, e.g., rhodium or platinum, X-ray energies up to and surpassing 30 keV will be covered with very high photon intensity at this grazing angle. For comparison, this mirror acceptance is simply not possible on an undulator or wiggler beamline on the existing NSLS X-ray ring. At best, such a mirror could intercept only about 15 % of the horizontal beam fan.

We expect that all NSLS-II macromolecular crystallography beamlines will employ undulator sources, allowing coverage of photon energies up to 30 keV with unprecedented brightness. The NSLS-II shield wall will be positioned at 25 meters from the source point, and our preliminary design is to position the monochromator/slit/filter assembly (double or four-bounce crystal monochromator based either on cryogenically-cooled silicon crystals or water-cooled diamond crystals) immediately thereafter, followed by a KB focusing mirror assembly. The KB mirrors will be outfitted with dynamical curvature adjustments that will allow them to a produce a micro-focus X-ray beam over a range of demagnifications from approximately 2:1 to ~10:1, depending on experimental requirements. The parameters of the KB mirror system are given in Table 4.1.1 and the optical arrangement is shown in Figure 4.1.1. A long experimental hutch will be used to provide sufficient space for a diffractometer and area detector, and will allow the instrument to translate along the beam path to permit use of different demagnifications while maintaining the sample at the focal position.

The expected "real world" performance of an NSLS-II undulator X-ray crystallography/scattering beamline employing a Si(111) double crystal monochromator and KB focusing optics is shown in Table 4.1.2. Blurring of the focal spot (calculated by ray tracing) due to an assumed mirror figure error of 0.5 μrad and transmission losses due to the monochromator, mirrors, and beamline windows have all been included in the estimated performance of the NSLS-II beamline in order to compare it to actual measured

Mirror Coating	Rhodium and/or Platinum			
Grazing Incidence Angle	3 mrad			
Operating Energy Range	~ 3 – 30 keV			
Efficiency of KB system at 12 keV	90% (Rh coating), 75% (Pt coating)			
VFM Length	30 cm			
HFM Length	80 cm			
	<u>High Demagnification Mode</u>		<u>Low Demagnification Mode</u>	
VFM (undulator-mirror distance, 30 m)	Focal Length	5 m	Focal Length	12 m
	Demagnification	6:1	Demagnification	2.5:1
HFM undulator-mirror distance, 31 m)	Focal Length	4 m	Focal Length	11 m
	Demagnification	7.75:1	Demagnification	2.8:1

Table 4.1.1 *KB system parameters for NSLS-II X-ray scattering/crystallography beamline. VFM is vertical focusing mirror, HFM is horizontal focusing mirror.*

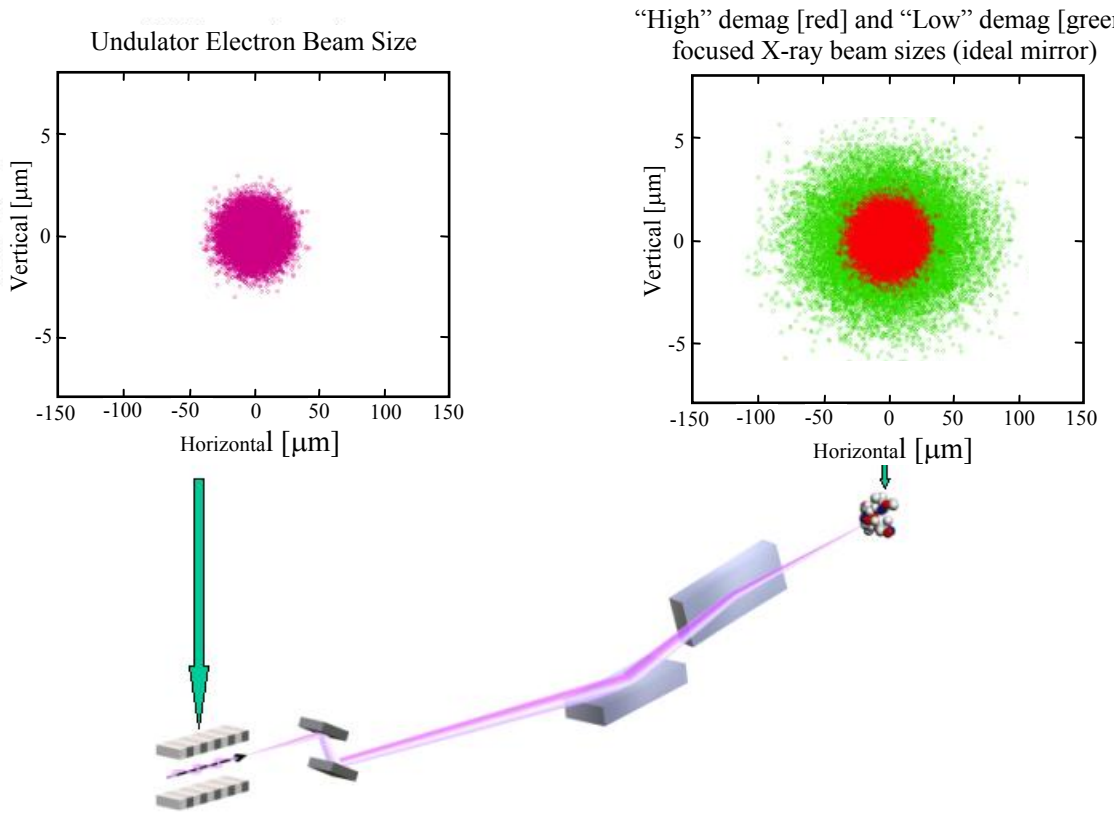

Figure 4.1.1 *Optical arrangement of the KB mirror system for an NSLS-II superconducting undulator X-ray scattering/crystallography beamline. Top-left plot: electron source dimensions. Top-right plot: high demagnification (red) and low demagnification (green) focused X-ray beam dimensions for ideal KB mirrors. A two bounce monochromator is placed upstream of the KB mirrors to enable energy selection.*

performance of beamlines at existing facilities. The existing beamlines listed for comparison in Table 4.1.2 are the NSLS X25 wiggler beamline, the new NSLS X29 undulator beamline that is under construction, and a typical "Undulator A" (UA) macromolecular crystallography beamline at the APS [1]

Undulator/Wiggler	NSLS X25	NSLS X29	APS UA	NSLS-II
Monochromatic flux at 12 keV (ph/sec)	$3x10^{12}$	$3x10^{12}$	$1.5x10^{13}$	$2.4x10^{14}$
Energy resolution w/ Si(111) (eV)	12	4	1.8	1.8
Vertical focus size, FWHM (μm)	200	100	30	11.9/28.5
Horizontal focus size, FWHM (μm)	700	250	60	27/77.5
Vertical convergence angle (mrad)	0.15	0.2	0.1	0.17/0.07
Horizontal convergence angle (mrad)	1.0	1.0	0.35	0.58/0.22
Monochromatic intensity at 12 keV (ph/sec/μm^2)	$2x10^7$	$1.2x10^8$	$8x10^9$	$7.5x10^{11}/1.1x10^{11}$

Table 4.1.2 *Expected "real-world" performance of an NSLS-II X-ray crystallography/scattering beamline (including 0.5 μrad mirror figure error and transmission losses for the monochromator, mirrors, and beamline windows) and comparison with actual performance of existing beamlines at the NSLS and APS. The expected performance for NSLS-II in both high and low demagnification modes of operation of the KB assembly is shown as high/low values.*

RMS mirror figure error [μrad]	0.0	0.1	0.5	1.0	2.0
Vertical focus size, FWHM (μm)	1.7 / 4.0	2.9 / 6.9	11.9 / 28.5	23.6 / 56.5	47.0 / 112.9
Horizontal focus size, FWHM (μm)	25.7 / 70.5	25.7 / 70.7	27.3 / 75.1	31.8 / 87.5	45.5 / 125.2
Monochromatic intensity at 12 keV (ph/sec/μm^2)	5.5x10^{12} / 8.5x10^{11}	3.3x10^{12} / 5.0x10^{11}	7.5x10^{11} / 1.2x10^{11}	3.3x10^{11} / 5.0x10^{10}	1.1x10^{11} / 1.6x10^{10}

Table 4.1.3 *Expected "real-world" performance of an NSLS-II X-ray crystallography/scattering beamline (including mirror figure error and transmission losses for the monochromator, mirrors, and beamline windows) for different values of mirror figure error. The expected performance in both high and low demagnification modes of operation of the KB assembly is shown as high/low values.*

(e.g. SBC-CAT, which is operational, and GM/CA-CAT, which is under construction). NSLS X25 and APS UA values are based on measurements, and the NSLS X29 data are expected values.

A critical physical parameter determining the image quality of the focused beam in the NSLS-II superconducting undulator beamlines will be the residual figure errors of the KB mirror surfaces. At the present state-of-the-art for fabrication of grazing-angle X-ray optics, the beam parameters at the focus of an ultra-low-emittance source such as the NSLS-II would be limited by aberrations resulting from this residual surface figure error. Indeed, one reason to keep the distance from these KB mirrors to the focus relatively short is to prevent their surface figure errors from contributing excessively to the focused spot size. On the other hand, we expect that the state-of-the-art in X-ray optics fabrication will continue to improve significantly between now and the start of NSLS-II operations [2-4]. Table 4.1.3 shows the expected improvement in focused X-ray beam parameters for the undulator X-ray beamline described above as a function of rms surface figure error of the KB mirrors in these beamlines. The perfect-mirror case (0.0 μrad figure error) is included as a point of reference. As was done for Table 4.1.2, transmission losses due to the monochromator, mirrors, and beamline windows were taken into account.

4.1.1.2 Small Angle X-ray Scattering

The small-angle X-ray scattering (SAXS) beamlines to be built for NSLS-II, schematically shown in Figure 4.1.2, will utilize a bendable KB focusing mirror pair for primary focusing and will have the flexibility of being tailored for different applications by using slits and secondary focusing mirrors.

Owing to the low emittance of NSLS-II, the full beam from the undulator will be able to be used for SAXS measurements down to very low q without any collimating slits. The divergence of the X-ray beam at the sample is limited by the acceptance angle of the KB mirrors and translates into a minimum accessible scattering angle (2θ) of 0.033 mrad. At an X-ray energy of 8 keV (7.4x10^{15} photons/sec/0.1%bw), the lowest q is ~1.4 x10^{-4} Å^{-1}, corresponding to 4.7 μm in real space. In practice, to

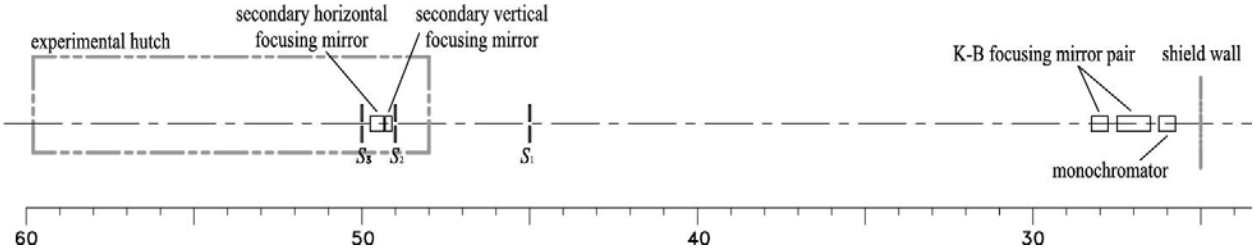

Figure 4.1.2 *Schematic design of the SAXS beamline. The beamline will be equipped with primary K-B focusing mirrors and two secondary cylindrical focusing mirrors. While the primary pair is sufficient for routine experiments, the secondary mirrors can be combined with the primary pair to provide the capability of grazing incidence scattering off liquid surfaces and SAXS within a spot size of a few microns.*

S_1 and S_2 (μm)	S_3 (μm)	Beam size at downstream end of expt'al hutch	Lowest q	Flux at the sample (ph/sec/0.1%bw)
100	150	2.2 mm @ 8 m	0.6×10^{-3} Å^{-1}	1.3×10^{15}
400	600	2.6 mm @ 2 m	2.8×10^{-3} Å^{-1}	7.0×10^{15}

Table 4.1.4 *Typical microbeam SAXS performance at 8 keV, assuming 1 μrad mirror figure error.*

S1 (μm)	S2 (μm) horizontal only	FWHM beam size (μm)		FWHM beam divergence (mrad)		Flux at the sample (ph/sec/0.1%bw)
		horizontal	vertical	horizontal	vertical	
200 (h) x 100 (v)	open	14	13	0.7	0.2	6.4×10^{15}
200 (h) x 100 (v)	200	13	13	0.5	0.2	4.0×10^{15}
50 (h) x 25 (v)	open	5	4	0.6	0.2	6.2×10^{14}

Table 4.1.5 *Typical microbeam SAXS beam size, divergence, and flux at the sample at 8 keV, assuming 1 μrad mirror figure error.*

achieve low scattering background and compensate for the divergence created by the figure error of the optical elements, collimating slits will be used (see Table 4.1.4).

Ideally, the secondary horizontal focusing mirror can further focus the full beam to under 10 μm (FWHM) in both horizontal and vertical extent at the sample, even without additional focusing in the vertical direction. Owing to the imperfection of the optical elements, a secondary KB focusing mirror pair will be used to obtain very small beam sizes. To do this, the primary KB pair focuses the beam at S_1 as a virtual source and the secondary mirrors then focus the beam again at the sample. Use of the variable aperture at S_1 to limit the size of the virtual source can further reduce the beam size at the sample. Typical performance values for a few selected choices of S_1 and S_2 slit sizes are shown in Table 4.1.5. By varying the figure of the secondary vertical mirror, e.g. by use of a tangential bender mechanism, one can also deflect the beam downward and focus it on a liquid sample cell (bath) in order to perform grazing incidence scattering measurements on liquid surfaces.

4.1.1.3 Nanoprobes

Several X-ray nanoprobe instruments are planned for NSLS-II undulator beamlines. These will provide unprecedented spatial resolution and intensity for imaging, diffraction and fluorescence based applications. X-ray nanoprobe beamlines are not significantly different from a standard X-ray scattering/crystallography beamline, described in Section 4.1.1.1. The main difference is that the optics are designed to focus the incident X-ray beam into nanometer sized X-ray spots at the expense of angular beam convergence on the sample.

Fluorescence and diffraction measurements differ in their requirements on the angular convergence of the photon beam on the sample: the fluorescence technique is insensitive to this, whereas the increased convergence due to the larger demagnifications delivered through the nanofocusing X-ray optics results in a broadening of the diffraction peaks from the sample and hence a reduced sensitivity to strain. The important figures of merit for X-ray nanoprobes are the focused beam size, angular convergence, total flux into the focused image, the ratio of flux in the focused spot to the unfocused background, and beam stability. These factors have to be carefully considered in the design of a nanoprobe instrument.

The emphasis for these beamlines will be obtaining high quality optics that conserve the source brightness and focus the beam to nanometer sized dimensions. Ten years ago the quality of focusing optics was such that a 5-10 μm spot was an expensive and heroic achievement. The present state-of-the-art X-ray optics employed at synchrotron radiation sources can deliver focused X-ray beams of order 100

nm using KB mirror systems [5, 6], diffractive zone plates [7] or refractive lenses [8]. As technological advancements continue, we believe that by the time NSLS-II is commissioned, these optics will be able to deliver X-ray nanobeams with dimensions of ~10 nm and below.

A variety of advanced optics for nanoprobes applications are described in Section 2.4.3.1. As a general rule, the absolute precision with which these demanding optical elements can be fabricated improves as the size of the optic decreases. The small aperture of current micro-focusing optics relative to the fan of radiation at existing, less bright sources such as the present NSLS means that they intercept only a small fraction of the source flux and hence the radiation is inefficiently utilized. The brightness of NSLS-II provides the important advantage that it will be a much better match to the acceptance of small, more precisely shaped, optical elements.

We also anticipate a complement of scanning transmission X-ray microscopes (STXM), which are rapidly becoming workhorses in the synchrotron radiation community. In the standard STXM configuration, the zone plate, which is 10-20% efficient, is located upstream, rather than downstream, of the specimen in the X-ray beam path, thereby minimizing the radiation dose to the sample. This minimization is particularly advantageous in the study of biological samples. STXM instruments are well suited to acquiring near-edge absorption spectra, both from specific points in a specimen and from whole image fields. The STXM user community at the NSLS has led the development of multivariate statistical analysis methods to exploit the information these spectromicroscopy data provide for studies in biological, soft matter, and environmental science [9].

The highest resolution microprobes now operating at NSLS (X1A1 and X1A2) are a pair of soft X-ray scanning transmission X-ray microscopes (STXMs) with a 36 nm Rayleigh resolution [10]. These microscopes are presently being equipped with laser interferometer feedback on the scanning stage motion, and are outfitted with unique segmented detectors that can be used to obtain both absorption and phase contrast images in a single scan. Since the present NSLS has a source phase space of about 100 λ horizontally and 3 λ vertically for 300 eV photons, the undulator source must be imaged to a secondary focus that is then apertured to deliver the required phase space area in the manner of a laser spatial filter. Moreover, the NSLS X1 undulator provides radiation to three endstations (STXMs at X1A1 and X1A2, and either soft X-ray diffraction or spectroscopy at X1B) simultaneously, so neither of the two STXMs is able to collect radiation from the on-axis undulator peak. The combined effects of off-axis viewing and efficiency losses from the additional optics required to re-image the source reduce the throughput of these microscopes considerably.

STXM-based soft X-ray research will benefit greatly from NSLS-II, which will provide ultra-high brightness in the soft X-ray range with 40 mm period Soft X-ray Undulators (SXU). The STXM beamlines will be based on spherical grating monochromators, which will be designed to demagnify the undulator source to an exit slit/pinhole in order to define the virtual source for the zone plate focusing optics. We propose to employ a pair of mirrors to direct the X-ray beam to one of two end stations, thereby allowing two microscopes to be operated in turn (or even in parallel if desired). By incorporating two microscopes in one SXU beamline, one of them can operate while upgrades or novel optical configurations are explored on the other (a pattern that has worked extremely well at the present X1A1 and X1A2 beamlines). In fact, since it is expected that the existing STXMs will be continuously upgraded between now and NSLS-II commissioning, these microscopes should be able to effectively make use of first light from NSLS-II.

4.1.1.4 High-resolution Inelastic X-ray Scattering

Inelastic X-ray Scattering (IXS) determines the scattering amplitude, $S(q,\omega)$, by measuring the intensity and energy loss of photons scattered by the sample into a small element in angular space. Ideally, the energy resolution of the monochromator and the analyzer are of the order of 1-100 meV, depending on the system under investigation. If the energy of the incident photons is tuned to an absorption edge of the sample, resonant processes can increase the intensity by a few orders of magnitude compared to non-resonant experiments. The cross section of IXS is fairly small, and including the

geometry of the experimental set-up, efficiency of detectors, and reflectivity of analyzer crystals, just 1 out of approximately 10^6 photons is detected if the white line is studied in resonant experiments using the K_α-fluorescence lines. Experiments in the pre-edge region lower the signal by another factor of 10-50 and studies using other fluorescence lines, K_β and K_γ, reduce the signal by another factor of 60-300. This reduces the signal in a typical experiment to $10^3 - 10^5$ photon/sec for an incident flux of 10^{12} photon/sec. Non-resonant experiments devoted to the study of band-gaps in insulators or semiconductors may even have count rates as low as 50 photon/sec and non-resonant experiments examining the absorption-edges of low Z elements (Raman scattering) will be of the order of 10^2-10^4 photon/sec for an incident flux of 10^{12} photon/sec.

The purpose of the high-resolution inelastic X-ray scattering beamline is to deliver highly monochromatic X-rays with a monochromaticity of 100 meV and 1 meV between 5 keV and 20 keV, large tunability, and highest possible intensity. A high resolution IXS instrument operating on an NSLS-II undulator beamline will be provided with a highly intense and extremely well-collimated source of X-rays, thus allowing the delivery of highly monochromatic X-rays with good efficiency. It is expected that a resolution of 10 meV will be achievable in the 5 to 20 keV photon energy range with a flux of about 10^9 photons/sec.

The main optical components of a high-resolution inelastic X-ray scattering beamline are similar to a conventional scattering beamline. The first optical component is a high-heatload cryogenically cooled monochromator that reduces the power on the optical components downstream, especially on the high-resolution monochromator. The bandwidth of this first pre-monochromator is on the order of 1-2 eV. To increase the efficiency of the high-resolution monochromator, the beam is collimated by a spherical mirror downstream of the pre-monochromator. Several different types of monochromators can be considered to obtain high monochromaticity of order either 100 meV or 1 meV, as shown in Figure 4.1.3.

The low-resolution (100 meV) monochromator can be either a four-crystal in-line [11-13] or nested monochromator with high-order reflections and a dispersive arrangement of reflections. Several monochromators of this type are already in use at various synchrotron radiation facilities around the world, and do not present any technical challenge. The loss in intensity due to the smaller energy width and the reflectivity of the crystals will be of the order of 50 compared to the intensity of the pre-monochromator. From Table 4.1.2, the Si(111) double crystal pre-monochromator will provide a monochromatic intensity at 12 keV of 2.4 x 10^{14} ph/sec with an energy resolution of 1.8 eV. Thus, we expect that the low-resolution monochromator will provide a flux of about 5 x 10^{12} ph/sec at 12 keV with an energy resolution of 100 meV.

The high-resolution (1 meV) monochromator for the energy range 5 to 20 keV with large tunability will be a technical challenge. Backscattering monochromators operating at Bragg-angles of 89.9^o have a small tuning-range of a few meV and operate only at specific high energies if Si-crystals are used [14]. Sapphire (Al_2O_3) significantly increases the tuning range and the energy-range, but so far, sapphire crystals of the required quality and size are not available. Nested monochromators can reach an energy-resolution of 5-10 meV with a tunability of a few eV, but only at a few energies close to the backscattering energies of specific reflections of Si [15-17]. A third option was recently proposed by

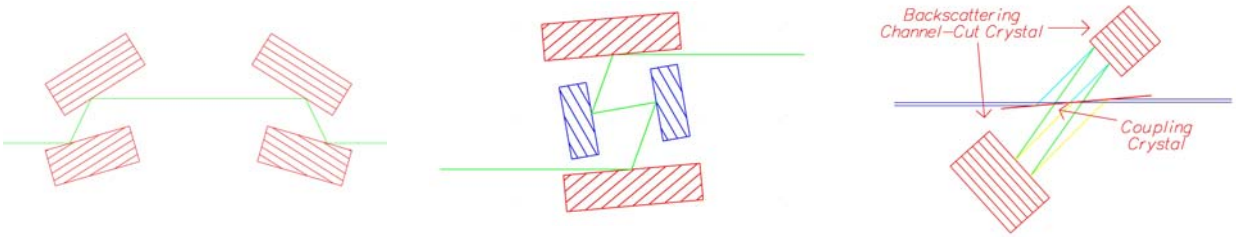

Figure 4.1.3 *Example types of monochromators for medium and high energy resolution for IXS applications. Left: In-line monochromator for medium energy resolution of 50-200 meV. Center: Nested monochromator for high energy resolution (5-10 meV). Right: Compact coupling-crystal backscattering monochromator for ultra-high energy resolution (0.5-1 meV).*

Shvyd'ko: Three crystals collimate the beam, monochromatize it, and focus it again. This arrangement has a theoretical energy resolution of about 1 meV with large energy tunability but has not yet been tested under real conditions. The loss in intensity from that provided by the pre-monochromator will be about a factor of 1000 due to the smaller energy-width, and an additional factor of 10 due to several additional reflections, so an intensity of ~ 2 x 10^{10} photons/sec at an energy resolution of 1 meV should be possible with this arrangement.

Downstream of the high-resolution monochromator in the IXS beamline, a pair of focusing mirrors (vertical and horizontal) is used to focus the beam onto the sample.

The spectrometer that analyzes the scattered X-rays with high energy resolution is another crucial part of the beamline. Several back scattering analyzer systems with energy-resolution of 100 meV (1 meV) using spherically bent analyzers with radii of curvature of 3 m (7-11 m) have demonstrated their high efficiency over the past decade [11, 16-19]. The future challenge will be to build a spectrometer that will be capable of determining the energy of scattered photons with high energy resolution at angles smaller than backscattering, e.g., the fluorescence lines of 3d and 4f elements, which are not close to backscattering energies of either Si or Ge reflections. One alternative might again be sapphire, but the availability of large perfect single crystals and its elastic properties pose a significant challenge. Again, the proposal by Shvyd'ko with an arrangement of a collimating mirror and three crystals (collimation, monochromatization, focusing) might be an interesting alternative, albeit one that is quite challenging for stability.

The analyzer system offers the only way to increase the signal by increasing its area and using separate detectors for each individual analyzer. Since each individual analyzer sees the scattered photons at a different scattering angle, each one measures its own $S(q_i,\omega)$, which will save time, and deliver the signal under identical conditions.

4.1.1.5 Superconducting-wiggler-based High Energy Beamlines

A small but important subset of the programs outlined in Section 2 have a need for high energy X-rays (e.g. > 30 keV) for X-ray scattering in order to probe a larger q range or to better accommodate special sample environments. A major advantage of using high energy radiation is the reduction in the absorption of X-rays, allowing the study of large samples and samples inside specialized environmental chambers. Focused high-energy X-rays are essential for high-resolution X-ray scattering of samples in multi-anvil and sometimes in diamond anvil cells, for larger q range, and to better accommodate the special high-pressure/temperature sample environment. Newly developed X-ray focusing optics and

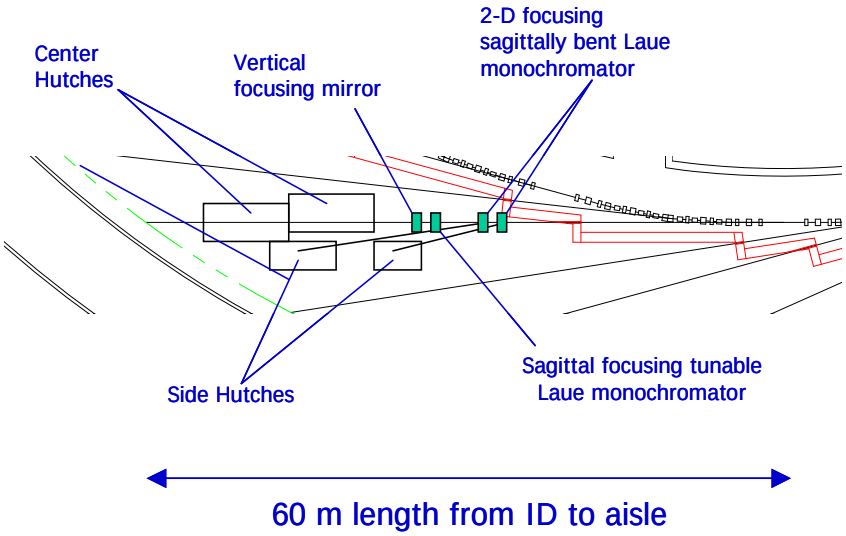

Figure 4.1.4 *Layout of NSLS-II superconducting wiggler beamlines.*

detectors are already poised to take advantage of the enhanced flux and brightness of the NSLS-II superconducting wiggler source to enable a myriad of crystallographic and spectroscopic measurements.

The superconducting wiggler beamlines will provide X-rays in the energy range 30 keV to 150 keV. At NSLS-II, the machine energy is 3 GeV, compared to 6 GeV, 7 GeV and 8 GeV respectively for ESRF, APS and SPRING8. Superconducting wigglers are therefore chosen to provide the desired high-energy X-rays. For wiggler radiation, the fan is about 10 mrad wide. Focusing of the hard X-rays is thus crucial to collect this large horizontal fan and utilize it for experiments.

Figure 4.1.4 shows a sketch of a possible arrangement for beamlines utilizing a high-field wiggler source on NSLS-II. The experimental stations include two fixed-wavelength side stations and two center stations that can utilize either white beam or focused monochromatic beam (or both).

Sagittal focusing using Laue crystals was pioneered at the NSLS [20-23]. The concept is shown in Figure 4.1.5. This new X-ray optics concept makes it possible to focus a large divergence of high-energy X-rays produced by the NSLS-II superconducting wiggler. The extent of such focusing is similar to that of sagittal focusing by a Bragg crystal, except for a factor related to the asymmetry angle. The anticlastic bending facilitates the use of inverse-Cauchois geometry in the meridional plane to provide better energy-resolution and to increase the photon flux by an order-of-magnitude compared to traditional sagittal

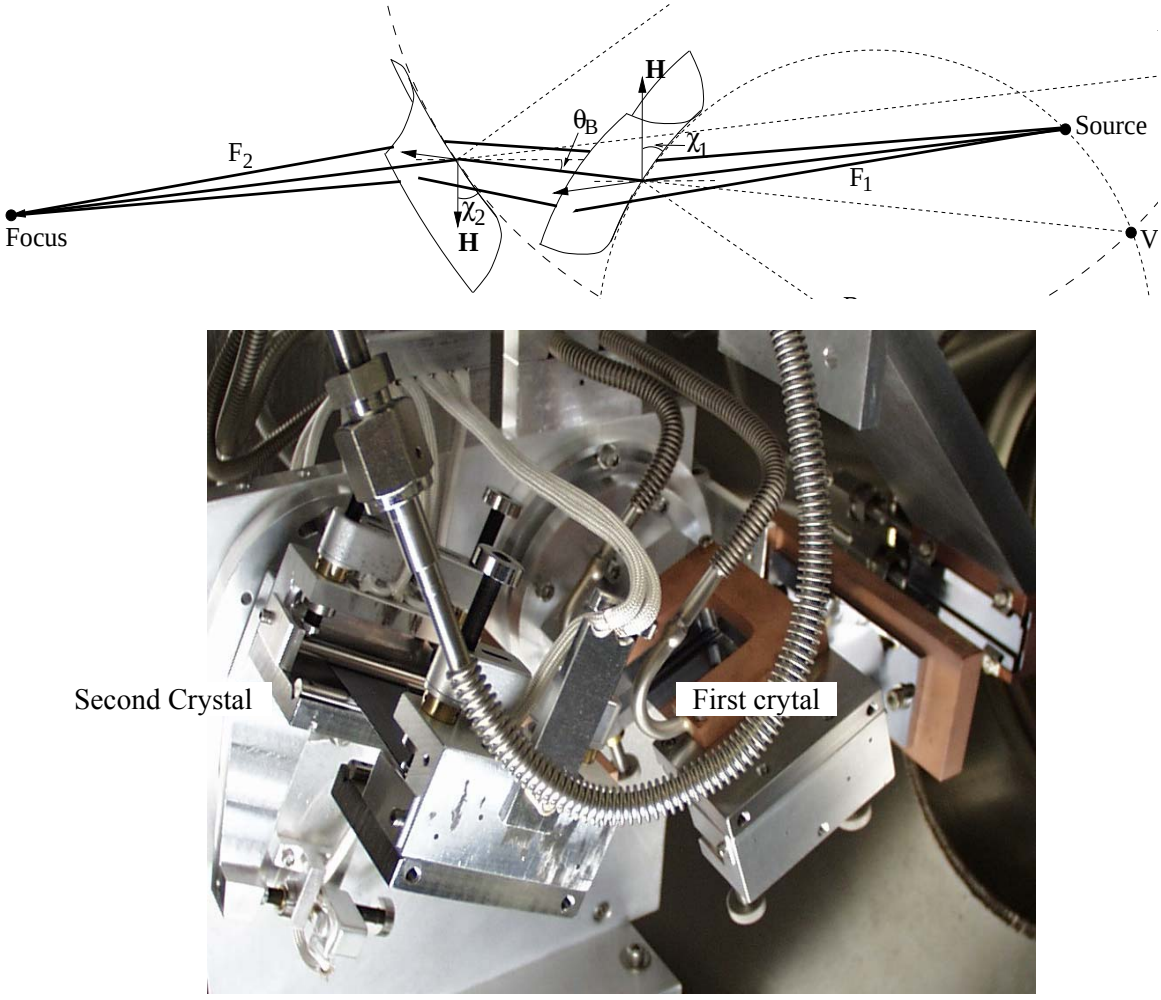

Figure 4.1.5 *Top: Schematic layout of the sagittal focusing mechanism using asymmetric Laue crystals. Bending of the crystals causes precession of the diffraction vector (H) around the axis of sagittal bending and results in focusing of the diffracted beams. Bottom: Photograph of such a monochromator installed at the NSLS X17B1 beamline.*

focusing with Bragg crystals. Furthermore, sagittal focusing by a Laue crystal is preferred over a Bragg crystal at X-ray energies above 30 keV because, since, unlike Bragg crystals, the length of the beam's footprint on a Laue crystal is small and insensitive to energy. For many experiments, beam divergences of order 1 mrad at the sample will be tolerable. For diffraction experiments in a vertical scattering plane, a larger divergence in the horizontal plane can also be tolerated.

A double-crystal sagittally focusing monochromator, based on this concept, has been constructed, tested, and in use at the X17B1 beamline for two years, providing 67 keV X-rays (Figure 4.1.5). It focuses a horizontal divergence of 3 mrad to a brightness-limited horizontal dimension of 0.2 mm. The X-ray flux density at the focus is a few hundred times larger than that of unfocused X-rays. Currently, using this device, the flux on a small sample in a diamond-anvil cell is limited by the brightness of the NSLS storage ring. Combined with a vertically focusing mirror, the same monochromator can be implemented at the NSLS-II superconducting wiggler beamlines to provide 50-100 keV photons of about 10^{12} ph/s, with an energy resolution of 10^{-4} $\Delta E/E$, in a spot of less than 50 microns in diameter. This intensity is two orders of magnitude larger than the current state-of-art at NSLS X17B1 and APS. For example, currently at APS 1-ID beamline, using bent Laue crystal optics that are best suited for the undulator, a flux of 10^{11} ph/s with an energy resolution of 10^{-3} is delivered to a similar spot of 100 microns in diameter at 67 keV [24].

The conditions imposed on the asymmetry angle of a sagittally bent Laue crystal to achieve two-dimensional focusing have been derived by NSLS scientists. This simple high-efficiency design diffracts high-energy X-rays into side stations providing a high-flux fixed-energy beam of 67 keV with moderate ($\Delta E/E \cong 10^{-3}$) energy resolution and a flux of $\sim 10^{13}$ ph/s/mm^2 in a spot of less than 50 microns vertical by 100 microns horizontal. This, when coupled with a matching bent-Laue crystal analyzer, allows high-resolution scattering experiments at high energies. This arrangement is suitable for pair distribution function measurements and powder diffraction measurements in difficult environments, e.g., stainless steel reaction tubes and high temperature capillaries. It will also be valuable for certain single crystal experiments such as charge density studies, where data must be collected to very high q values.

The use of white radiation and energy sensitive detectors for energy dispersive diffraction is an established technique for kinetic experiments in high pressure (large volume press) and high temperature experiments. With the optical elements withdrawn from the center beam, the end station will accept white radiation, thus allowing for energy dispersive experiments.

4.1.2 Soft X-ray Beamlines

The 4.0-cm period, 5.0m-long soft X-ray undulator (SXU) provides high brightness radiation in the soft and intermediate X-ray ranges, from 0.2-7 keV. This large photon energy range will naturally lead to a combination of grating-based and crystal-based beamlines in order to provide efficient utilization.

Above 2.5-3.0 keV photon energy, the range where crystals function robustly and efficiently, the extremely narrow angular width of the central cone emission from the SXU will not overfill the angular acceptance of the highest quality crystals. Furthermore, sagittal focusing will not be required of these crystals, since reasonable-length focusing mirrors will still collect the entire central cone even at 30-40 m meters from the source point (see Section 4.1.1.1). Depending on the application, either single mirror or Kirkpatrick-Baez pair designs will be used to refocus the diffracted radiation onto the sample.

Below 2.5-3.0 keV photon energy, the domain of grazing-incidence diffraction gratings, the extremely high brightness of the SXU beam will provide a very efficient source for the grating, whether it should be real (i.e. focused through an entrance slit) or virtual (e.g. in the SX700 monochromator design [25]). The maturation of variable-line-space grating technology and the superior control over groove shape now provided by the grating manufacturers has pushed the resolving power of soft X-ray monochromators well beyond 10^4 while also providing a fixed exit position and angle [26]. The advent of accurate bendable gratings [27] provides another variable parameter to the soft X-ray monochromator

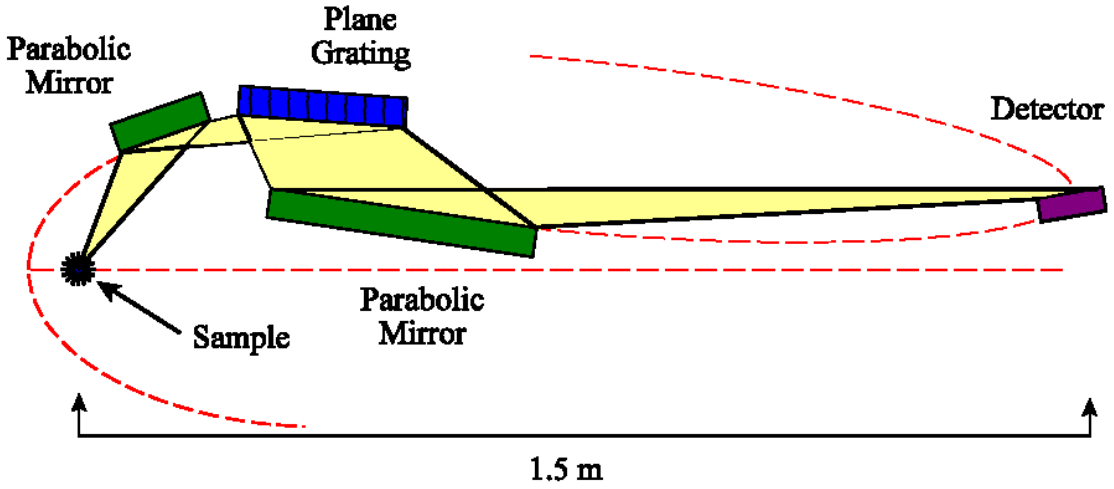

Figure 4.1.6 *Soft X-ray emission spectrometer.*

designer. The magnification of the monochromator does not differ greatly from unity, so the design of the refocusing mirror(s) is similar to the double-crystal cases above: either a single asphere or a KB pair.

The tiny vertical extent of the refocused monochromatized SXU beam incident on the sample will create a source of soft X-ray emission that will be an ideal match to high-resolution soft X-ray emission spectrometers. One such spectrometer is that being designed by Josef Nordgren (Uppsala) (Figure 4.1.6), in which scattered 50-200 eV soft X-rays from the sample are collected by a parabolic mirror and collimated onto one of three interchangeable plane gratings. The diffracted X-rays are focused by a second parabolic mirror onto a micro-channel-plate detector. This instrument should be able to achieve the super high resolution of < 10 meV at a photon energy of 75 eV. It is, however, a very brightness-hungry instrument, requiring micron-sized beams on the sample since the photon beam on the sample acts as a virtual entrance slit for the emission spectrometer. Thus, the high brightness of NSLS-II in the soft X-ray energy range is essential in order for this instrument to reach its full capability.

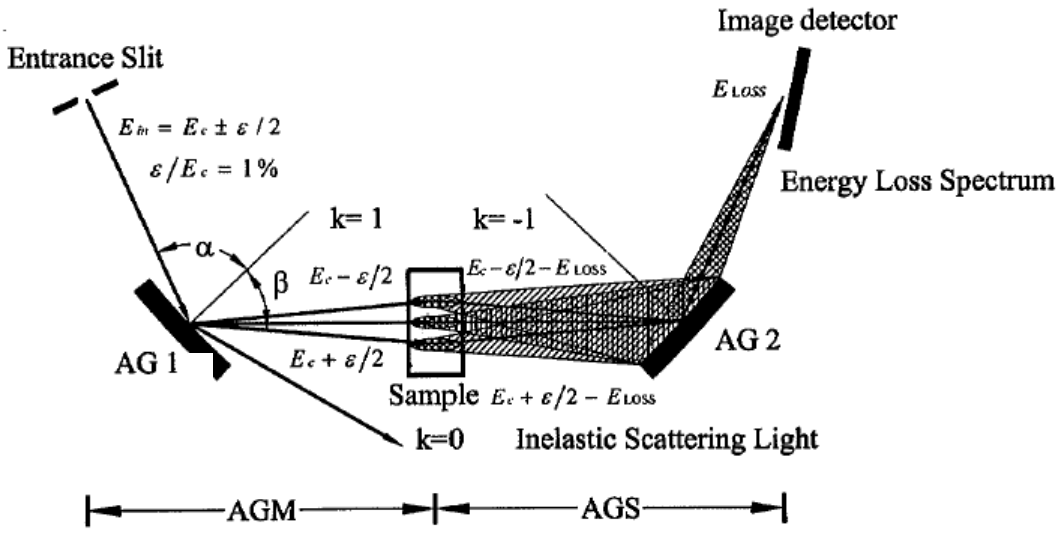

Figure 4.1.7 *Conceptual diagram of the SRRC parallel-detection soft x-ray emission system. The active grating monochromator (AGM) and active grating spectrometer (AGS) are time-reversed images of each other, thereby compensating aberrations to achieve high energy resolution.*

The SXU will also be an ideal source for the newly designed [28] dispersion-compensated combination of soft X-ray monochromator and soft X-ray emission spectrometer, shown in Figure 4.1.7. This world-leading design, to be commissioned in 2004, will greatly increase the effective count rate of soft X-ray emission spectroscopy by acquiring an entire energy-loss spectrum at once, i.e. without having to scan either the beamline monochromator or the emission spectrometer.

4.1.3 High-K-undulator-based VUV Beamlines

Despite the hard X-ray critical energy (7.8 keV) of the NSLS-II X-ray storage ring, the VUV (10-100 eV and above) users will be served very well by long-period high-K undulators (See Figure 3.3.3). These insertion devices could be either planar or of a more exotic magnetic structure such as the Figure-8 [29] or Pera [30] designs. One advantage, especially for the planar high-K undulator, is the very large photon energy range covered by the first, third, and fifth harmonics: from ~10 eV to 1 keV. Thus, high resolution spectroscopy will be able to be performed over a very wide energy range at one endstation, a capability desired by both XPS and angle-resolved photoemission spectroscopists. The disadvantage of high-K planar undulators is the associated extremely high power levels, both total power and angular power density. This power load may be compatible with modern integrally-cooled optics, albeit with some degradation owing to the inevitable thermally-induced surface figure error on the first beamline optical element. One attractive solution to this problem is the Figure-8 undulator design, or similar variants such as the Pera design, in which the high energy harmonics are for the most part missing in a narrow cone on axis that encompasses the low harmonics (e.g. first, third, and fifth). In this case, the first beamline element is a cooled circular aperture that acts as a cost effective energy filter, allowing only the relatively low power but very high brightness fundamental and next few harmonics to pass.

The design of beamlines for these 10-1000 eV sources must necessarily involve combinations of monochromators, each of which covers only a fraction of this range with optimized parameters. For example, the 10-40 eV photon energy range requires a normal incidence monochromator (NIM) design in order to achieve high resolution with high throughput, whereas the 40-1000 eV range can be handled by any of the high-resolution soft X-ray monochromator designs. With careful consideration to proper layout, both the VUV and soft X-ray monochromators can be served alternately by the same undulator source and their output beams directed to a common focused spot on the sample. The achievable resolving power in both the VUV and soft X-ray range continues to increase as the quality of optics, in particular diffraction gratings, improves. In the VUV range, NIM monochromators can achieve well above 10^5 resolving power [31]. In the soft X-ray range, resolving powers are above 10^4 over large ranges of photon energy, and approaching 10^5 at particular photon energies.

4.1.4 Infrared

Infrared synchrotron radiation (IRSR) serves a diversity of scientific disciplines in biology, chemistry, materials, physics, geology, environmental and space sciences. As a source, IRSR spans the entire range from 1 cm^{-1} up to 4000 cm^{-1} (and beyond) with characteristics that enable measurements that otherwise would be impossible [32]. The key aspect to infrared synchrotron radiation is the high brightness (2 to 3 orders of magnitude higher than conventional laboratory spectroscopy sources) that allows throughput limited experiments to be performed with ease. A primary example of this is infrared microspectroscopy, where synchrotron radiation extends the spatial resolution by about 1 order of magnitude (to the diffraction-limit) while still delivering high signal-to-noise. Many other techniques have similar throughput limitations, e.g. ellipsometry, precision reflectance spectroscopy, and grazing incidence reflection spectroscopy, all of which have restrictions placed on the acceptable angle of incidence at the specimen. Techniques such as high-pressure spectroscopy and magnetospectroscopy are constrained by the instruments and their limited optical access. Lastly, a high brightness source is necessary to achieve proper modulation (absence of skew rays) over the very large path lengths of a high-

resolution spectral resolution interferometer. Each of these throughput limited techniques are problematic at mid-infrared frequencies and become increasingly difficult as the spectral range reaches into the very far-infrared and THz region. Infrared synchrotron radiation has overcome some of these problems and efforts continue to improve the source capabilities, especially at the more difficult long-wavelength end of the spectrum.

Another less exploited quality of IRSR is the pulse structure that can be used in time-resolved studies of dynamics [33]. Though the pulse duration (10s to 100s of picoseconds) is significantly longer than what can be achieved with ultra-fast lasers (10s to 100s of femtoseconds), the synchrotron is a "white" source that allows complete spectral information to be acquired. This provides a unique opportunity to study dynamics associated with chemical bonds (vibrational spectra), both charge transfer and interband electronic transitions, and even intraband absorption (by free carriers) all in a single experiment.

Many of the scientific programs described in Section 2 require a high brightness, white source of pulsed infrared – the characteristics which the NSLS-II IR ring described in Section 3 will excel at.

The infrared beamlines will be designed to span the spectral range from about 0.5 eV (4000 cm^{-1}) down to 10 meV (80 cm^{-1}), and in some cases to as low as 250 μeV (2 cm^{-1}). The NSLS presently offers a suite of 6 infrared beamlines, several of which are heavily oversubscribed. The IR community is also among the fastest growing user communities at the present NSLS. Thus, we anticipate expanding this to at least 8 to 10 beamlines on the NSLS-II IR ring to meet the great demand for high brightness, short pulse, broad spectrum IR radiation.

Currently we envision beamlines serving the following scientific needs:

- Materials at extremely high pressure and temperatures (diamond anvil cells)
- Biological microspectroscopy and imaging.
- Environmental and Space materials (microprobe spectroscopy, including far-IR).
- Far-infrared magnetic resonance spectroscopy in high fields
- Fast material dynamics / time-resolved IR spectroscopy
- Precision reflectance spectroscopy and ellipsometry of new and complex materials
- Custom microscopy configurations for nanomaterials, quantum wells and quantum dots.

The useful spectral range is often limited by the extraction port dimensions, rather than downstream optical components (and even the spectrometer endstations). Therefore, the ports for infrared beamlines will all be as large as practical (at least 90 $mrad^2$). This is particularly important for reaching into the THz spectral range, an area of increasing interest. At least two beamlines will be optimized for performance in this low frequency range. The technology for providing radiation at THz frequencies is rapidly evolving, and accelerator-produced THz pulses are no exception. The proposed long wavelength beamlines will be compatible with such technologies as they become available.

REFERENCES:

[1] R. Fischetti, private communication

[2] D. Hausermann et al., *Synchrotron Radiation and Instrumentation 2003 Conference Proceedings, San Francisco, Ca, 2003, in press*.

[3] R.Signorato and T. Ishikawa, Nuclear Instruments and Methods in Physics Research A (467-468), 271-274, 2001.

[4] P. Eng et al., *Test Results of GSECARS Large KB Mirror Focusing System*, http://cars9.uchicago.edu/gsecars/mirrors/index.html

[5] Hignette, G. Rostaing, P. Cloetens, A. Rommeveaux, W. Ludwig, A. Freund, Proceedings of SPIE, X-ray Micro- and Nano Focusing: Applications and Techniques II, 105-116, 2001.

[6] Hignette, P. Cloetens, W.-K. Lee, W. Ludwig and G. Rostaing, J. Phys. IV France 104, 231-234, 2003.
[7] W.Yun, B. Lai, Z. Cai, J. Maser, D. Legnini, and E. Gluskin, Rev. Sci. Instrum. 70, 2238-2241, 1999.
[8] C.G. Schroer, M. Kuhlmann, U.T. Hunger, T.F. Gunzler, O. Kurapova, S. Feste, F. Frehse, B. Lengeler, M. Drakopoulos, A. Somogyi, A.S. Simionovici, A. Snigirev, I. Snigireva, C. Schug and W. H. Schroder, Appl. Phys. Lett. 82 (9) 1485-1487, 2003.
[9] C. Jacobsen, M. Feser, M. Lerotic, S. Vogt, J. Maser, and T. Schäfer, Journal de Physique IV **104**, 623 (2003). M. Lerotic, C. Jacobsen, T. Schäfer, and S. Vogt, Ultramicroscopy (submitted).
[10] M. Feser, C. Jacobsen, P. Rehak, and G. De Geronimo, Journal de Physique IV **104**, 529 (2003).
[11] Y.Q. Cai, P. Chow, C.C. Chen, H. Ishii, K.L. Tsang, C.C. Kao, C.T. Chen, Optical Design and Performance Of The Taiwan Inelastic X-ray Scattering Beamline (BL12XU) At SPring-8, Proceedings of the Eight International Conference on Synchrotron Radiation Instrumentation, San Francisco, California, August 25-29 2003.
[12] G. Faigel, D. P. Siddons, J. B. Hastings, P. E. Haustein, J. R. Grover, J. P. Remeika and A. S. Cooper, Phys. Rev. Lett. 58, 2699-2701 (1987)
[13] W. A. Caliebe, C.-C. Kao, M. Krisch, T. Oversluizen, P. Montanez, and J. B. Hastings, AIP Conference Proceedings, Volume 417, 6-9 (1997).
[14] R. Verbeni, F. Sette, M.H. Krisch, U. Bergmann, B. Gorges, C. Halcoussis, K. Martel, C. Masciovecchio, J.F. Ribois, G. Ruocco, and H. Sinn, J. Synchrotron Rad. 3, 62-64, (1996).
[15] Alfred Q. R. Baron, Yoshikazu Tanaka, Daisuke Ishikawa, Daiwo Miwa, Makina Yabashi, and Tesuya Ishikawa, J. Synchrotron Rad. 8, 1127-1130, (2001).
[16] Tetsuya Ishikawa, Yoshitaka Yoda, Koichi Izumi, Carlos Kenichi Suzuki, Xiao Wei Zhang, Masami Ando, Seishi Kikuta, Rev. Sci. Instrum., 63, 1015-1018, (1991).
[17] E. Ercan Alp, H. Sinn, A. Alatas, W. Sturhahn, T. Toellner, J. Zhao, J. Sutter, M. Hu, D. Shu, Y. Shvydko, Nucl. Instr. and Meth. in Phys. Res. A, 467-468, 617-622, (2001).
[18] C. Masciovecchio, U. Bergmann, M. Krisch, G. Ruocco, F. Sette, R. Verbeni, Nucl. Instr. And Meth. in Phys. Res. B, 111, 181-186, (1996).
[19] C. Masciovecchio, U. Bergmann, M. Krisch, G. Ruocco, F. Sette, R. Verbeni, Nucl. Instr. and Meth. in Phys. Res. B, 117, 339-340, (1996).
[20] Z. Zhong, C.C. Kao, D.P. Siddons and J. B. Hastings, J. Appl. Cryst. 34 (2001) 504-509.
[21] Z. Zhong, C.C. Kao, D.P. Siddons and J. B. Hastings, J. Appl. Cryst., 34 (2001) 646-653.
[22] Z. Zhong, C. Kao, D.P. Siddons and J.B. Hastings, Acta Cryst, A 58 (2002) 487-493.
[23] Z. Zhong, C. Kao, D.P. Siddons, H. Zhong, and J.B. Hastings, Acta. Cryst. A 59 (2003) 1-6.
[24] S.D. Shastri, K. Fezzaa, A. Mashayekhi, W.K. Lee, P.B. Fernandez and P.L. Lee, *J. Syn. Rad.* **9** (2002) 317-322.
[25] H. Petersen, C. Jung, C. Hellwig, W.B. Peatman, and W. Gudat, Rev. Sci. Instrum. **66**, 1 (1995).
[26] M. Koike and T. Namioka, Rev. Sci. Instrum. **66**, 2144 (1995), and references therein.
[27] T.C. Tseng, D.J. Wang, S.Y. Perng, C.K. Kuan, J.R. Lin, S.H. Chang, and C.T. Chen, J. Synchrotron Radiation **10**, 450 (2003).
[28] H.S. Fung, C.T. Chen, et al., "A Novel Active Grating Monochromator – Active Grating Spectrometer Beamline System for Resonant Inelastic Soft X-ray Scattering Experiments", in the proceedings of the 8th International Synchrotron Radiation Instrumentation Conference, San Francisco, CA, 2003.
[29] T. Tanaka, H. Kitamura, Nucl. Instrum. Methods **A364**, 368 (1995); T. Tanaka, H. Kitamura, J. Synchrotron Radiation **3**, 47 (1996).
[30] S. Sasaki, B. Diviacco and R. P. Walker, "Brainstorming on New Permanent Magnet Undulator Designs", in proceedings of the 1998 IEEE Particle Accelerator Conference, Stockholm, Sweden.
[31] C. Masciovecchio, D. Cocco, and A. Gessini, "Inelastic Ultra-Violet Scattering as a Tool to Investigate Collective Excitation in Condensed Matter Physics", in the proceedings of the 8th International Synchrotron Radiation Instrumentation Conference, San Francisco, CA, 2003.

[32] G. L. Carr, P. Dumas, C. J. Hirschmugl, and G. P. Williams, Nuovo Cimento, 20D, 375 (1998).
[33] R. P. S. M. Lobo, J. D. LaVeigne, D. H. Reitze, D. B. Tanner, and G. L. Carr, Rev. Sci. Instrum. 73, 1 (2002).

4.2 Extreme Sample Environments

A major challenge in the physical sciences is to expand our understanding of nature by finding new material phases that are predicted to occur, such as quantum critical phenomena and exotic correlations. Very often, this requires tuning parameters such as pressure, magnetic field, and temperature to extreme values to access the novel phenomena. We intend to equip NSLS-II with associated facilities for obtaining as extreme of environments as possible in synchrotron experiments so that one can perform structural and spectroscopic studies that are not possible at non-synchrotron-based facilities. Our plans for providing experimental facilities at NSLS-II to attain world leading extremes of pressure, magnetic field, and temperature are described in this Section.

4.2.1 High Pressures

Ground-breaking high-pressure experiments reveal numerous new phenomena. We are at the exciting moment when high-pressure research is emerging to become a major branch of modern science. The high-pressure environment drastically and ubiquitously alters all material properties, thus opening new frontiers in fundamental physics and chemistry, as well as applications to planetary, Earth, biological, and materials sciences.

To investigate novel phenomena in-situ in high-pressure environments, powerful probes must be developed to reach minute samples through the strong wall of the pressure vessel and to separate the weak sample signals from those of the surrounding vessel materials. High-energy synchrotron radiation enjoys a unique advantage in this regard, as other conventional methods are unsuitable. For instance, pressure vessels are impenetrable by electrons or VUV to soft X-ray photons; on the other hand, the spatial resolution and intensity of conventional X-ray or neutron sources is insufficient for accurate studies at megabar pressures. A vast frontier has opened for high-pressure synchrotron radiation applications. The symbiotic evolution of high pressure and synchrotron radiation science has produced bountiful results in the past and showed boundless future for scientific exploration.

Parallel to three generations of synchrotron radiation advances, the marriage of high pressure environments with synchrotron facilities has also gone through three distinctive phases. At the beginning in the 1980's, users brought high pressure cells loaded with samples and experimental hardware and software, including X-ray optics, sample-handling stage, diagnostic probes, detectors, etc., to basically empty hutches at synchrotron facilities. Research projects were limited by the relatively primitive instrumentation that could be brought in, set up, and dismantled afterward within the assigned beam time.

Figure 4.2.1 *Megabar diamond anvil cell with natural diamonds sitting on the penny, and an anvil representative of the next generation of synthetic diamonds.*

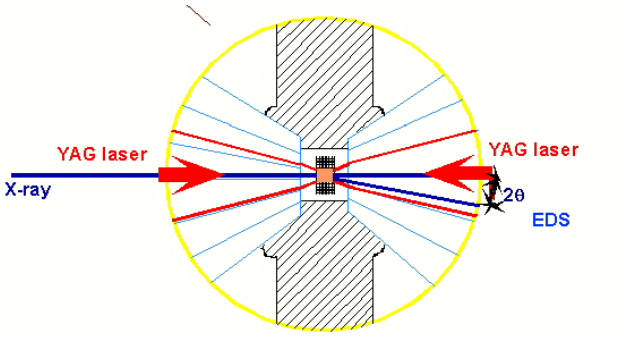

Figure 4.4.2 *Arrangement for heating sample at high pressure. Focused laser beams are capable of creating temperatures of several thousand K.*

Nevertheless, exciting pioneering results demonstrated the potential (e.g., pressure-induced amorphization, metallization, and diffraction of ultralight elements, ultrahigh-pressure diffraction above 300 GPa). In the 1990's, single-task (X-ray diffraction) beamlines were constructed and dedicated for high pressure experimentation at X17 of NSLS, ID9 and ID30 of ESRF, and other synchrotron facilities. Dedicated high pressure beamlines allowed the establishment of multianvil apparatus, high-precision diffraction systems, and combined high pressure and high temperature environments that required years to build and optimize, and enabled the extraordinary scientific growth that we have witnessed. In the current decade, the multitasked HPCAT sector at APS combines myriad compatible and complementary synchrotron diffraction and spectroscopy techniques for dedicated high P-T studies. This comprehensive and integrated approach is enabling the next level of advancement.

All existing high-pressure/synchrotron radiation programs, however, were developed after the completion of the synchrotron rings. Consequently, they were restricted by the preset, backward conditions. For the first time, we now have the rare opportunity to plan high pressure synchrotron science for the next decade at NSLS-II. We will be able to consider high pressure as a key sample environment and build an overall infrastructure that combines high pressure with high temperature, cryogenic, and high magnetic field environments. We may build an ideal high pressure synchrotron radiation program that includes both HPCAT-type, multitask beamlines optimized for extensive sample environments and single-task beamlines optimized for special X-ray techniques, but accommodating the P-T-magnetic field conditions. Most importantly, the forward-looking infrastructure can incorporate next-generation high pressure devices.

Major breakthroughs in high pressure technology that will completely change the status quo are looming on the horizon. For instance, high pressure synchrotron studies have been previously limited to small access angles in the forward-scattering geometry. With the invention of panoramic diamond-anvil cells, the nearly complete spherical coverage of reciprocal space and momentum space has become accessible for single-crystal X-ray diffraction and inelastic studies. With the improvement of transparent beryllium and diamond gaskets, the conventional wisdom that only high-energy photons significantly above 10 keV could penetrate the high pressure vessel has been changed. Inelastic X-ray scattering has eliminated the blind spot between 5 eV and 5 keV where the high pressure vessels were opaque, and has opened the full, continuous range from meV to 100 keV. Micro- and nano-diffraction and spectroscopy allow us to investigate the elasticity and rheology of single grains as small 100 nm at multimegabar pressures. On the other hand, the development of giant CVD single-crystal diamonds holds the promise of mm-size sample volumes, 1 eV temperatures, and multimegabar pressures. As high pressure X-ray, high pressure neutron, and related initiatives (e.g., HPCAT, SNAP, COMPRES, and CDAC) continuously push the envelope, these breakthroughs will enable a new generation of scientific advancement in the high-pressure environment that will require considerably different planning than in previous high pressure synchrotron facilities.

The next five years will see continued developments in this area coupled with the creation of new high-pressure devices capable of higher pressures, larger sample volumes, hydrostatic sample conditions, higher and lower temperatures, and multiple analytical probes. These developments will allow measurements to be carried out to the most extreme conditions with an accuracy, precision, and sensitivity approaching studies at ambient conditions. Most important is an initiative aimed to increase sample size at megabar pressures using new gem anvil technology. Depending on the hardness of the gemstones, maximum pressures of 16.7, 25.8, 52, and 300-550 GPa have been reported for cubic zirconia, sapphire, moissanite, and diamond anvils, respectively. The transparency of gem-quality, diamond single crystals over a wide range of the electromagnetic spectrum -- including X-rays, ultraviolet, visible light, and most of the infrared -- permits the application of an unusually large number of complementary analytical techniques for probing samples at multimegabar pressures. This transparency makes it also possible to introduce laser beams that can heat samples from ambient temperature up to electron volt range while at multimegabar pressures.

The fabrication of large, perfect single-crystal diamond using high-growth rate chemical vapor deposition (CVD) stands to revolutionize the field of high-pressure research with the prospect of creation of large perfect anvils employed in a new generation of high-pressure cells. X-ray diffraction measurements carried out at the NSLS indicate that the CVD diamonds can generate multimegabar pressures. Moreover, high P-T annealing of single-crystal CVD diamond has produces material that is significantly harder than any other diamond-based material. Vickers hardness and fracture toughness tests show that the annealed CVD diamond is ultrahard (>160 GPa), beyond that of both type IIa natural diamond and polycrystalline diamond. This ultrahard CVD diamond, together with its high growth-rate synthesis, should find a variety of applications beyond high-pressure technology.

4.2.2 High Magnetic Fields

To address the broad range of topics which require extreme magnetic fields for their study, a dedicated beamline with a state-of-the-art high-field steady state magnet will be built. A picture of one of the high field magnets in use at the current NSLS is shown in Figure 4.4.3. The much smaller source size of the high brightness NSLS-II ring will allow a smaller vertical split, increasing the highest attainable field strength. Existing technology should make it possible to build a vertical-field split-coil superconducting magnet with a maximum field of 20 Tesla or more (at present, the largest field at a synchrotron source is 15 T at Spring-8). Most of the systems of interest mentioned in Section 2 can be successfully studied using such a magnet. The magnet should possess a large bore to allow use of sample environment devices (such as high-pressure cells), temperature range of at least 0.3-300 K (or higher T), and windows suitable for small-angle scattering and inelastic experiments (low background). An additional consideration that will be taken into account is to make the windows with as little absorption as possible for lower energy resonant scattering experiments.

The beamline will be equipped for general diffraction, resonant diffraction, and common X-ray spectroscopy techniques, such as XAS. In certain cases, somewhat smaller field magnets will be available on dedicated specialized beamlines, for example small angle scattering, to complement the large field techniques. These combined capabilities will form a unique experimental facility, both in terms of the available magnetic field, and in terms of the broad range of the available experimental techniques.

Finally, we note that in high magnetic field research, no field is ever “high-enough” – new opportunities continually arise as the field is increased. It is clear that today the highest conceivable DC field compatible with a scattering experiment is the 20 T proposed here. Nevertheless, there are routes to higher fields, in particular through pulsed magnets, which can reach 60 T for periods of milliseconds. Such facilities will be highly desirable and will make an important contribution on the world scene to high-field research. It is envisioned that an auxiliary laboratory might be built to provide such fields, taking advantage of the high brightness beams from NSLS-II to bring X-rays into the adjoining laboratory, perhaps 100 m from the source, and carry out pump-probe experiments.

Figure 4.4.3 *The superconducting magnet installed at X22B, NSLS. At NSLS-II, steady-state magnetic fields 20 T or more will be available on a beamline with more than two orders of magnitude more flux than at X22B, allowing entirely new classes of problems to be studied.*

4.2.3 Ultra-Low Temperatures

At NSLS-II, a program in ultra-low temperature physics is anticipated, focusing in particular on scattering techniques, including resonant and non-resonant magnetic X-ray scattering, to address these and other questions. A dilution refrigerator will be installed as a dedicated end-station with appropriate technical support, such that routine operation in the 300 mK range will be available to users. There are significant heat load problems that will need to be solved in order to reach such temperatures at NSLS-II. These problems will be addressed in a pilot program which has already begun at the present NSLS in a collaboration between the NSLS, Lucent Technologies, and the Advanced Photon Source.

4.3 Automation and Robotics

New Synchrotron Facilities are being faced with an ever increasing number of users whose principle focus is not on synchrotron radiation methods. A typical example can be found in the bio-molecular, bio-medical community, which is driving the automation process in the field. These researchers employ synchrotron radiation as a routine tool in their research.

To meet the needs of this community, the structure determination process must be streamlined. A production pipeline for high volume determination of structures requires optimization and automation of current processes in use at synchrotron facilities. The ultimate goal is to arrive at a system that, with little more input than a sample, will provide the researcher with the final molecular structure.

Structure determination by X-ray diffraction is a procedure that involves multiple steps, from beam alignment to sample handling, data acquisition and finally model building. Several groups have been addressing the sample environment, data processing and model building [1]. To expedite sample exchange, which can take from 5 to 30 minutes per sample, robotic sample exchangers have been under development at several synchrotron facilities and are now also commercially available. The goal is to put in place an end-to-end, sample-to-structure, automated bio-molecule characterization capability (Figure 4.3.1).

Automated systems with emphasis on remote access and control have been in development and use for several years at different facilities. The so called FEDEX, or MAIL IN, system developed by the structural biology group in the BNL Biology Department for their NSLS stations has found success with users who do not want to spend the time or money to travel to a Synchrotron Facility to collect their structural data. The main goal of the Material Microcharacterization Collaboration [2] is to provide researchers with a virtual laboratory at their home institutions that will allow the ultimate characterization of their samples at different member laboratories over the internet. The mission of the CmolS, an X-ray diffraction collaboration for research, education and training funded by the W.M. Keck Foundation [3] is

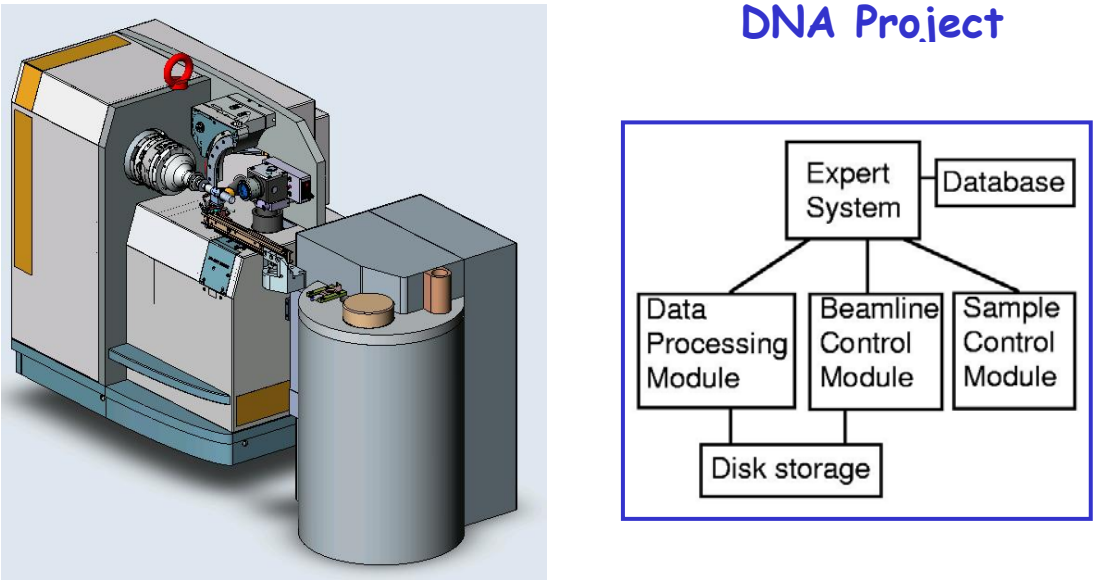

Figure 4.3.1 *The first step towards high sample throughput in structural biomolecular crystallography community was driven by Structural Genomic Initiatives. The goal is to arrive in the future to an end-to-end sample-to-structure, automated bio-molecule characterization machine. Shown here is a sketch of the Microdiffractometer and Automated Sample Changer developed by the EMBL (European Molecular Biology Laboratory) and the ESRF (European Synchrotron Radiation Facility) to be operational on the Protein Crystallography beam lines at the ESRF in 2004.*

to provide faculty and students with the opportunity for joint research and teaching activities directed at the determination of molecule structures. At the present NSLS, a first step towards an end-to-end molecular structure determination facility is to integrate an automated sample changer with a neural network pattern recognition algorithm to control the quality and the radiation damage to bio-molecular crystals [4].

To address the users' demands, the NSLS-II beam lines will incorporate fully automated controls. This will be achieved in two parts: one addressing the automated alignment of the optical elements in the beam line, and another addressing the full automation of the end-station, data collection, and data analysis; the goal is an end-to-end characterization capability. A possible approach is to design, demonstrate, and deploy a two layer system in which the top (artificial intelligence) layer reasons symbolically about what the monitoring and diagnostic sensors are saying about the state of the alignment, and the bottom (procedural control) layer translating these into a set of actuator adjustments needed to align the system. This approach will be used at as many facility beamlines as practical. Even though end-stations may differ in specifics, most are fitted with a series of sensors, mechanical slits, and rotation and translation stages, and can profit from sharing development efforts. For example, automated sample changers developed for structural biology end-stations will be adapted to sample changers for other sample intensive methods such as EXAFS or powder diffraction.

Several groups in Europe are collaborating to fully automate protein crystallography beam lines. In the DNA project [5], groups from ESRF, Daresbury, and Diamond are collaborating to develop prototypes of an automated data acquisition system, as shown in figure 4.3.1. In collaboration with the Trieste synchrotron, R. Pugliese developed a fuzzy logic expert system for beam line alignment. This system has been tested only with a toroidal mirror as optical element [6]. At Diamond and Soleil synchrotron facilities, the inclusion of beam line automation is under consideration.

Recently the explosion observed in the development of new technologies applied to the construction of ever smaller and smarter sensors and micro-machines has lead to second generation MEMS (micro-electro-mechanical systems) devices where automation is a requisite. Monolithically-Integrated MEMS devices allow for an independent integrated IC and passive/mechanical component design with an integration complexity similar to board level designs. Current MEMS applications include optical devices, mirrors, collimators and alignment aids; sensors and actuators, shutters, rotation and translation stages; electromagnetic devices, motors, solenoids and generators. The combination of several devices can lead to complex applications such as a MEMS micro-microscope shown in Figure 4.3.2.

Further technological developments aim to integrate a complete sensor/communication system into a cubic millimeter package. The goal of the "Smart Dust" project, initially developed by Kris Pister at UC Berkley [7], is to pack in a device the size of a grain of sand, sensors, computational ability, bi-directional wireless communications, and a power supply. While the goal is to attain a 1 mm^3 size device the current state-of-the-art Smart Dust devices are of the order of one hundred cubic millimeters.

Beam lines at the NSLS-II will be designed to take full advantage of the state-of-the-art developments in the area of artificial intelligence, robotics, neural networks, and sensor development. In broad strokes, it is possible to envision that the "Smart Beam Line" architecture would include a top layer based on artificial intelligence and pattern recognition systems and a bottom layer composed by sensors and actuators. The artificial intelligence layer will be used to handle tasks such as sample alignment, beam line control, and data collection and analysis. It will work concurrently with pattern recognition systems that will monitor the quality of data based on the actual images such as the diffraction pattern or beam profile. This top layer will control the beam line elements using actuators and sensors based on emerging technologies that include elements developed in MEMS and Smart Dust.

The challenge that lies ahead is to establish clear development paths for each of these components and the communication protocols between them. Expert systems and neural network techniques can be developed and implemented at the present time at existing beam lines. Collaborations with computer science and robotics research groups will be established to accelerate this development. User input and feedback will be crucial to the development and will provide the ultimate benchmark. The situation in the actuator and sensor front is slightly different and may require an aggressive development path. Devices

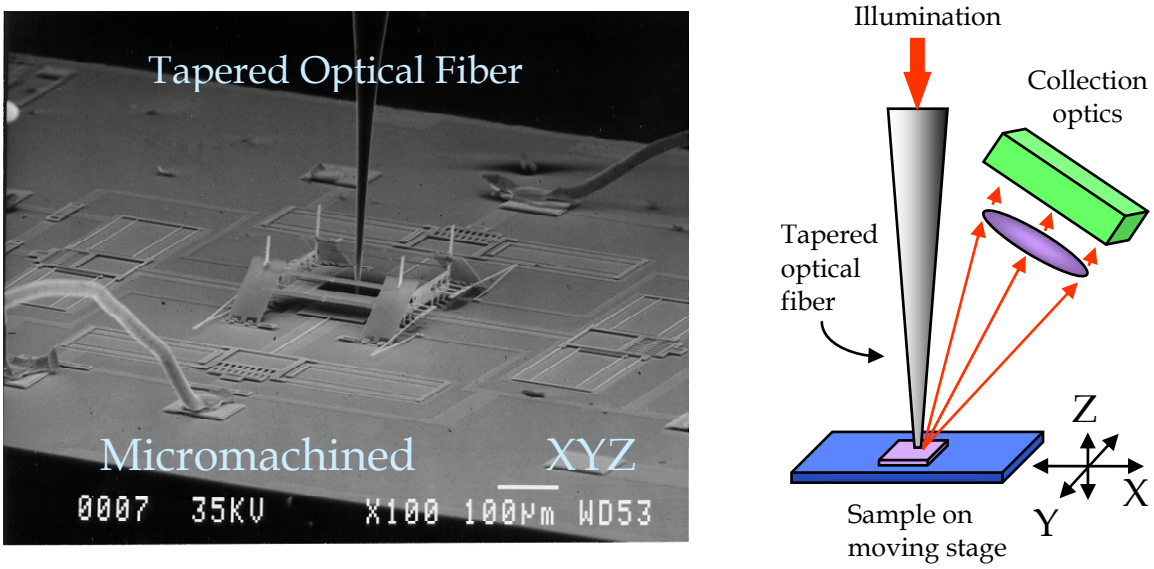

Figure 4.3.2 *MEMS micro-microscope; (a) Scanning Electron Microscopy of an XYZ stage (b) schematics of the micro-microscope [8].*

such as Smart Dust are being developed for general applications and specific development for beam lines may be required. Ionizing radiation, vacuum operation, and cryogenic temperatures may lead to custom development. However use of these new technological devices is not essential to the implementation of the "Smart Beam Line". Conventional actuators such as linear motors with ¼ micrometer precision are available today and are being further developed to attain higher precisions.

Finally, the "modus operandi" for the beam lines needs to be established. The data acquisition and data analysis will be controlled by the artificial intelligence layer and will provide at least a preliminary analysis of the collected data. In this sense the user may or may not be present physically at the beam line while data are being collected.

Taken together, development and use of these approaches at NSLS-II will set a new standard for beamline automation and control and facilitate high throughput usage of NSLS-II.

REFERENCES

[1] Interdisciplinary Workshop promoting collaboration in High-throughput X-ray Structure Determination, march 22-23, 2002, Santa Fe, NM, USA.
[2] http://tpm.amc.anl.gov/MMC/
[3] http://www-structure.llnl.gov/scaurcon99/cmols2.html
[4] Berntson, V. Stojanoff and H. Takai, "Application of a neural network in high-throughput protein crystallography", Journal Synchrotron Radiation (2003) 10, 445-449.
[5] http://www.dna.ac.uk/ and http://www.e-htpx.ac.uk/
[6] http://www.aps.anl.gov/conferences/icalepcs/97/paper97/p146.pdf
[7] http://robotics.eecs.berkley.edu/~pister/SmartDust/
[8] David Bishop, Lucent Technologies, private communication.

4.4 Detectors

4.4.1 Overview

Advanced detector systems will be required to take full advantage of NSLS-II's superlative performance. For a synchrotron experiment, the detector system is an especially critical component that often enables new science. One outstanding example is that of macromolecular crystallography. When the only viable area detector capable of quantitative interpretation was film, macromolecular crystallography was an esoteric pursuit, involving an exorbitant amount of labor to wet-process thousands of films for each experiment. The availability of synchrotron radiation sources made little impact. The development of new, large area, electronic detectors have transformed macromolecular crystallography into a high-throughput research powerhouse, providing key knowledge for the understanding of disease mechanisms and drug design.

4.4.2 Advances

4.4.2.1 Architecture

In general, it is clear that the trend is towards higher levels of functionality integrated into the detector elements and readout systems. This will include digital signal processing (DSP) of the analog sensor output as well as digital post-processing of events. These trends are already visible in the high energy physics field, and are beginning to be seen in synchrotron radiation systems. We can expect that pulse-height histograming, time and space correlations and spectral corrections will all be integrated at the chip level in future detectors.

Conventional computing resources are also beginning to be embedded in more application-specific integrated circuits (ASICs). At least one programmable gate-array device manufacturer is selling a product with up to four PowerPC processors embedded in the center of a large programmable gate array. In the 10 year process leading to NSLS-II, even more powerful devices can be expected. It is now almost as easy to embed a CPU into an ASIC as it is to include a subroutine in a software program. Modern simulation programs can accurately simulate the performance of a complete ASIC before manufacture, giving a high degree of confidence that the final device will work as specified.

More sophisticated devices will inevitably lead to increased data rates. This is already a limitation for existing detectors, particularly those that deal with images. Add to the large pixel count, the need for energy spectra and/or time-correlation spectra per pixel, plus the need for tomographic information, data set sizes can easily expand to terabytes. It is not yet clear how to handle the gigabyte/second data rates expected from the next generation of area detectors, so these more sophisticated devices will need real innovation in data movement technology, or a great deal more customizing of readout systems to reduce data in real time, probably using the embedded intelligence described above. A more detailed discussion of these issues follows.

Current detectors suitable for acquiring single-crystal and powder diffraction images are rather slow, with readout times of order one second or more. This aspect of 2-dimensional position-sensitive detectors is receiving significant attention due to the large ready market offered by macromolecular crystallography. If we imagine a modest device, with its readout rate increased one thousand fold, i.e. readout times of order 1 millisecond, with 2000 x 2000 pixels, we can see that we will rapidly saturate almost all present computer systems in digesting the 8 Gb/second that it will generate. Fortunately, such detectors will also be highly parallel in nature, in contrast to current charge-coupled device (CCD) technology. Thus, it should be a straightforward (but not simple) strategy to increase the number of CPUs dedicated to its readout. The combined FPGA/CPU device mentioned above is ideally suited to this task. Its FPGA could be programmed to accept and sort the raw data streaming from each column ADC and placed in local memory for later downloading or local processing. If we assume 8 ADC's per processor,

with each ADC digitizing at 2 MHz (a modest value, but consistent with low-noise operation) and providing 2 bytes per conversion, then we would require 256 FPGA/CPU chips to handle the 2048 columns, each one reading out the data at 32 Mb/second. If each CPU is provided with 1 Gb of local memory, then they could hold 32 seconds of data. The 256 systems would hold a total of 256 Gb of data.

It is impractical to move this amount of data around, so the most logical thing would be to analyze it in situ. This may seem like complexity for its own sake, but its potential impact could be huge. Many of the crystals studied by soft-condensed matter and biology scientists are extremely radiation-sensitive. The radiation damage is often diffusion driven and could be alleviated by reducing the total exposure time. The system described above could collect an entire data set in under one second, and a great many systems could survive this long, even at room temperature. This could remove the need to develop a freezing strategy for each new crystal, and could produce better data since the freezing operation lowers the crystalline perfection of most organic materials. It would be impractical to collect such data by collecting discrete frames, as is currently the fashion. Instead the sample would rotate continuously and the data would be read out continuously. Part of this local post-processing would be to unscramble these data streams to provide peak intensities and pattern indexing. Ideally, the output of such a detector would be I(h,k,l), the integrated intensities of all of the peaks, rather than raw images; a much smaller data set.

Another big advantage of such a detector readout scheme would be that it would have an arbitrarily large dynamic range. Present framing detectors have a finite capacity per pixel. This is currently mitigated by essentially throwing away signal (by using an X-ray phosphor and collecting the visible light very inefficiently) such that a full pixel corresponds to 10^5 – 10^6 X-ray photons. The noise level of such a system is at the 5-50 X-ray photon level. Direct detection of X-rays by a CCD typically results in a full-well of only 100 - 1000 X-ray photons, but the noise level is much less than 1 photon. The proposed XAMP detector full well corresponds to 10^4 X-ray photons. Reading out this detector continuously (e.g.,. every ms) would allow an instantaneous per-pixel rate of 10^7/s, and acquisition could continue as long as needed to provide the required statistical precision for the weakest signals.

As coherence becomes more a part of data collection strategies, detectors designed to measure efficiently the various correlations, spatial and temporal, will be required. One might expect that experiments traditionally considered small-angle scattering (SAXS) will become speckle experiments with the new source, providing dynamic structural information as well as static. The current state of the art provides single-point time correlation measurements down to the microsecond scale, and multipoint measurements at the 10 millisecond scale. The wish is for microsecond scale multipoint measurements, or even faster in the future. The ideal detector for such tasks is the fully-pixellated detector, although prototype experiments are currently carried out using other types of detector. This will have complete readout electronics for every pixel. The simplest system for generating correlations is a photon-counting system, but integrating systems should be able to adopt similar strategies if the intensity prohibits photon counting. Each photon will be tagged with its position and time coordinates. Time autocorrelation will be performed by on-chip logic, following one of the various multiple-time-domain algorithms to provide correlation information over the widest possible time scales. For large numbers of pixels and high count rates this will be the only possible approach. Spatial and temporal cross-correlations will be a much bigger challenge, since the interconnection scheme becomes highly complex. To date there are no examples of such systems outside of high-energy physics. NSLS-II will provide beams with a high degree of spatial coherence. In fact it will be diffraction-limited at 0.1 nm in the vertical plane. So-called speckle experiments will be greatly facilitated by this source, but full utilization will only come with the new detectors discussed here.

Pixel detectors equipped with energy-resolving capability will require the ability to put a complete energy-histogramming subsystem on each pixel of a large array. Such detectors will be the logical extension of devices currently reaching the experimental floor, which have hundreds of pixels each with a complete signal-processing chain. These systems were designed for fluorescence detection in absorption spectroscopy experiments with dilute samples, when the experiment feasibility is dominated by the presence of a high parasitic flux of uninteresting radiation. This results in premature saturation of the detector chain, enforcing long acquisition times and eventually preventing a successful experiment. This

situation will be worse with NSLS-II, and so we must plan for remedies. Increasing the parallelism even further is one way forward, and on-chip intelligence to deconvolve acquired spectra on a photon-by-photon basis will be a significant enhancement, bringing enhanced separation between the desired and parasitic radiation.

One could also imagine such a detector bringing a new lease of life to the Laue diffraction technique, since it becomes much simpler to perform the necessary diffracted intensity corrections if one knows the energy of the photon directly. This same knowledge also helps in indexing Laue patterns, and removes the problem of harmonic overlap. Nevertheless, fabrication of such a detector is no simple undertaking. A high-speed ADC is power-hungry, and one would need about 1 million of them for a reasonably sized detector. As CMOS technology continues to shrink, this will eventually be possible, at least for pixels of dimension 100 micrometers or more. Applications of such a detector might be in microbeam grain-mapping of polycrystalline materials, or high-pressure diffraction experiments. Such studies are important to provide a firmer basis for understanding the properties of real materials on all scales, and are ideally suited to a machine like NSLS-II.

4.4.2.2 Sensors

Currently, the highest performance detector elements are based on pure elemental semiconductors, either silicon or germanium. This is true across the detector spectrum, and is largely a consequence of the high commercial value semiconductor devices have yielded, with the consequent large investment in materials and processes. Sensor technology that is currently considered esoteric will become routine in the next decade, so we can anticipate high-speed devices with good energy resolution based on charge drifting techniques in large arrays, probably up to the sizes currently offered only by CCD devices.

Figure 4.4.1 shows a prototype 384-element array of drift-detectors that is part of a BNL development currently underway. These devices provide enhanced energy resolution by minimizing the capacitance seen by the amplifier by drifting the charges through large distances within the bulk of the silicon to a small collection electrode. It also illustrates another important aspect of silicon-based technology: the ability to make essentially arbitrarily shaped sensor arrays. The one illustrated will have a central hole. This allows an incident probe beam to pass through the detector and impinge on a sample. The scattered radiation is then efficiently detected by this array since there is no restriction on how close the detector can come to the sample. Thus a large fraction of the full sphere of radiation can be collected, even though the array is not very large (the pixels are 1mm diameter). It is simply an engineering problem to add further detector planes around a sample to increase even further the collection efficiency.

Various schemes are under development to provide rapid-readout area detectors for time-resolved studies. These range from intermediate solutions involving a reduction of the readout time to one dimension, similar to active matrix computer screens, all the way to dedicated per-pixel parallel readout

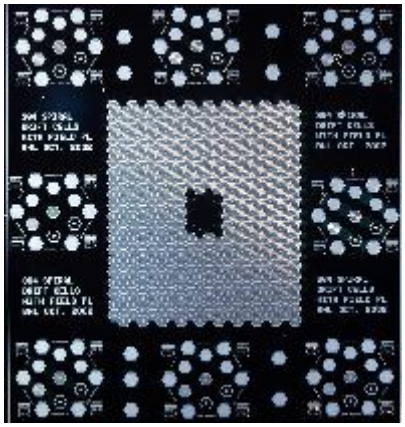

Figure 4.4.1 *Prototype 384-element array of drift detectors.*

of a sensor array typically separate from the readout array. Such devices will offer readout times less than one millisecond for active matrix devices, to a few microseconds for pixel arrays. Some of the issues with such devices are discussed above. We will surely see these developments continue and bear fruit. We will also see the next level of development where each pixel is also a spectrometer. The difficulties there are more of an engineering nature than any fundamental constraints.

Silicon is only useful up to energies of 15 keV or so, but the thrust of much of detector related materials science research is moving up towards 30 keV and more. Germanium is suitable for this range, but requires cryogenic technology, which is very restrictive. Cadmium Zinc Telluride is a promising material for room-temperature operation in non-spectroscopic applications, but it suffers from material problems that are proving difficult to overcome. Other high-Z semiconductor compounds are also under active development, GaAs or HgI for example. Such materials are particularly attractive in the context of pixel array detectors, where the ability to tailor the sensor properties for the radiation being detected will be valuable. Since the sensor array and the readout electronics are separate objects connected by flip-chip or bump bonding, both components can be optimized for the job in hand. This bonding technique, illustrated in Figure 4.4.2 is still in its infancy and much work needs to be done to make large detector arrays a reality.

A truly new detector principle is making its appearance based on superconductivity. There are two basic types, microbolometers and tunneling junction detectors. Each has its good points and its problems, but they both offer energy resolution in the eV range, with the bolometers having a slight advantage in resolution and energy range, but losing in count rate capability to the tunneling junction devices. Both types are physically small and hence have poor detection efficiency and low solid angle, but it is anticipated that large arrays will eventually be feasible that will mitigate most of these problems. Optimized readout ASICS have yet to be developed for such detectors, but even now they have achieved close to their theoretical limits, and have begun to be used for soft X-ray spectroscopy applications with excellent results. They operate at temperatures below 1 degree Kelvin, and so require advanced cryogenic techniques for their operation. Nevertheless, a reasonably portable and easily-operated tunneling junction device has been made at LLNL and has been used at synchrotron sources. It is shown in Figure 4.4.3.

4.4.2.3 Readout Electronics

Currently, CMOS is proving to be the most valuable technology for detector developers, since it is capable of both relatively high-speed digital and low-noise analog functions on the same chip. Current technology is 0.18 micron design rules (roughly the size of the smallest feature that can be fabricated), but

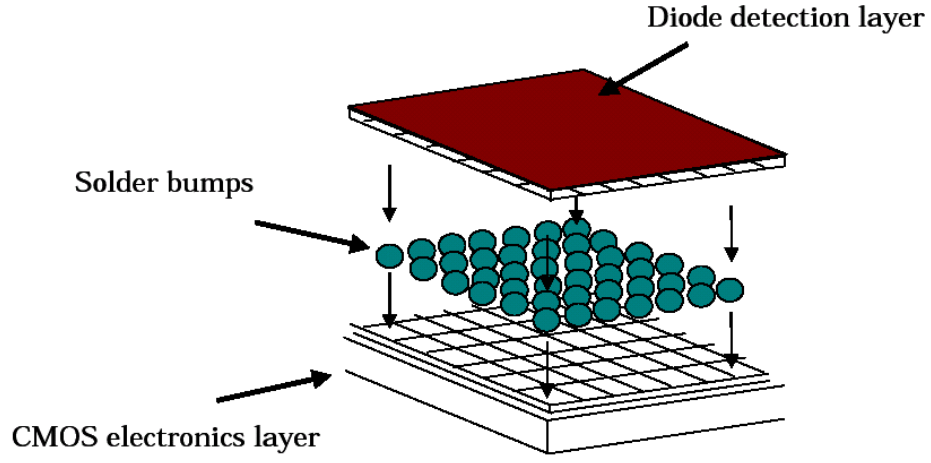

Figure 4.4.2 *Illustration of the bump bonding, a high density interconnection technique which makes possible so-called Pixel Array Detectors, where each pixel is directly connected to its own readout circuit in an underlying CMOS electronics layer.*

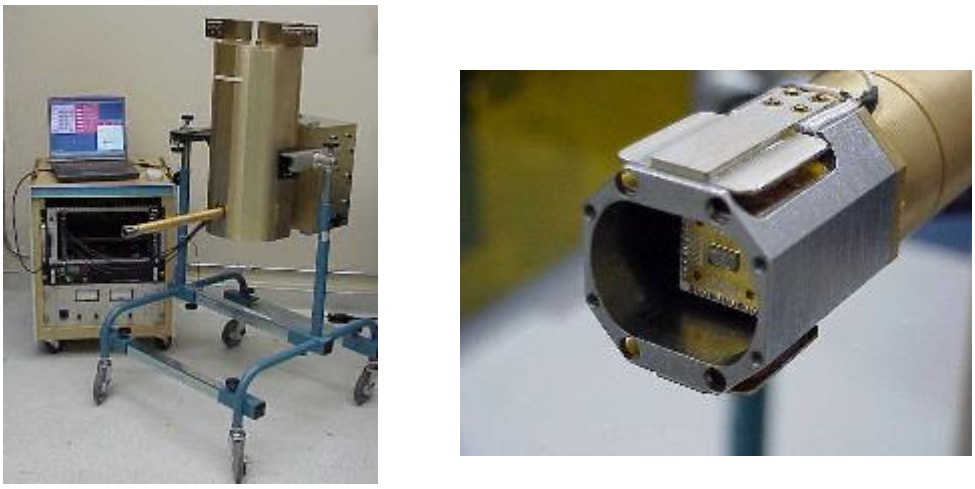

Figure 4.4.3 *Prototype superconducting tunnel junction detector, which offers eV energy resolution and high count rate capability.*

it will inevitably decrease. Although the analog circuitry consumes a lot of real estate that will not reduce as rapidly as digital circuitry due to the need for large capacitors, digital circuitry real estate diminishes as the square of the design-rule dimension. Thus a 0.18 micron circuit can pack four times the circuitry of a 0.35 micron device, with reduced power consumption and higher operating speed.

4.4.2.4 Software

There is an almost insatiable need for application software to bring advanced detectors to the point of being an asset in an experiment, rather than an experiment in its own right. A well-designed user interface can make possible experiments that would otherwise not be attempted. A good example is a scanning X-ray microprobe. In this experiment a small X-ray spot is raster-scanned over the surface of a sample, and an X-ray emission spectrum acquired at each point. Analysis of this three-dimensional data set (x, y, energy) is time-consuming and error-prone. Add to this a multi-element detector with perhaps thousands of channels and anything but an automated system becomes unthinkable. It is in principle possible to perform the analysis in an automated way, adjusting each element's setting for optimal operation, collecting reference spectra and then deconvolving the instrument function and providing elemental mapping corrected for background and peak overlap, on a photon-by-photon basis.